1) Over a relatively short monitoring period turbidity currents were active in Bute Inlet at various scales; these events resulted in channelized sand transport over low bottom gradients and long distances.

2) Individual flow events exhibited downfjord reduction in velocity and thickness but were sufficiently energetic to carry fine sands 40 to 50 km to the basin.

3) Flow thicknesses exceeded channel depth, both where the channel is deeply incised and on the outer bends of the channel below station 2. Between stations 1 and 2 the basal parts of the flow are channel confined, but upper levels may occupy the entire fjord floor, much in the manner indicated by Hay *et al.* (*4*).

4) Suspended sediment concentration (ρ) associated with the thickest parts of flows can be estimated from

$$CU^2 = g(\Delta\rho/\rho)h \tan B$$

(U is velocity, C is the drag coefficient, h is thickness, g is acceleration caused by gravity, and B is bottom slope). If C is 0.003, the average sediment concentration through the flow thickness is 12 g/liter. But this value is extremely sensitive to the drag coefficient. If C is 0.075 (*10*), the concentration is about 200 g/liter.

5) The factors responsible for the initiation of flow are not yet fully understood. The delta front is periodically unstable, and landslide generation of the turbidity currents is strongly suspected. Moreover, the association of one event with a major river flood raises the intriguing possibility that high bedload concentrations may be sufficient to generate sand suspensions, which continue downfjord along the bottom.

6) Bute Inlet offers a perfect natural laboratory in which to investigate the dynamics of active sand-transporting flows and elongated fan development. This depositional geometry is analogous to many ancient fans on active margins (*11*). The occurrence of similar channel depositional systems in neighboring fjords in British Columbia, such as Toba Inlet, provides opportunities for comparative studies.

REFERENCES AND NOTES

1. F. Weirich, *Sedimentology* **33**, 263 (1986).
2. B. C. Heezen, D. B. Ericson, M. Ewing, *Deep Sea Res.* **1**, 193 (1954).
3. W. R. Normark, D. J. W. Piper, D. A. V. Stow, *Am. Assoc. Pet. Geol. Bull.* **67** (no. 9), 1400 (1983).
4. A. E. Hay, R. W. Burling, J. W. Murray, *Science* **217**, 833 (1982).
5. A. J. Bowen, A. R. Normark, D. J. W. Piper, *Sedimentology* **31**, 169 (1984).
6. D. B. Prior *et al.*, *Geology* **14**, 581 (1986).
7. J. P. M. Syvitski, K. W. Asprey, D. A. Clattenburg, G. D. Hodge, *Sedimentology* **32**, 83 (1985).
8. J. J. Clague, S. G. Evans, J. G. Blown, *Can. J. Earth Sci.* **22**, 1492 (1985).
9. R. Y. Anderson, *Limnol. Oceanogr.* **22**, 423 (1977).
10. J. R. L. Allen, *Principles of Physical Sedimentology* (Allen & Unwin, Boston, 1985).
11. W. R. Normark and N. E. Barnes, *Geo-Mar. Lett.* **3**, 223 (1983–1984).

12. Supported by the Geological Survey of Canada and by National Science Foundation grant DPP-8501118. We thank W. Schroeder for suggesting significant improvements in the design of vane deflectors. We thank the master and crew of the *Vector* and I. Frydecky, L. Spearing, K. Conway, B. Blaise, R. Fredericks, and G. Liebzeit for providing invaluable technical support. Contribution 16887 of the Geological Survey of Canada.

17 March 1987; accepted 28 May 1987

Accelerated Healing of Incisional Wounds in Rats Induced by Transforming Growth Factor–β

THOMAS A. MUSTOE, GLENN F. PIERCE, ARLEN THOMASON, PEGGY GRAMATES, MICHAEL B. SPORN, THOMAS F. DEUEL

The role of polypeptide growth factors in the processes of inflammation and repair was investigated by analyzing the influence of transforming growth factor–β (TGF-β), applied directly to linear incisions made through rat dorsal skin. A dose-dependent, direct stimulatory effect of a single application of TGF-β on the breaking strength of healing incisional wounds was demonstrated. An increase in maximum wound strength of 220 percent of control was observed at 5 days; the healing rate was accelerated by approximately 3 days for at least 14 days after production of the wound and application of TGF-β. These increases in wound strength were accompanied by an increased influx of mononuclear cells and fibroblasts and by marked increases in collagen deposition at the site of application of TGF-β. TGF-β is thus a potent pharmacologic agent that can accelerate wound healing in rats.

GROWTH FACTORS PRESENT IN SERUM and platelet extracts are considered to play important roles in inflammation and wound healing (*1–3*). The platelet-derived growth factor (PDGF) and platelet factor 4 at low concentrations were first shown to be chemotactically active for human monocytes, neutrophils, smooth muscle cells, and fibroblasts (*4, 5*) and to stimulate inflammatory cells and fibroblasts (*6*), activities which indicated that these proteins were important in inflammation and repair. Another polypeptide growth factor, transforming growth factor–β (TGF-β), originally identified in conditioned media from transformed cells (*7*), was subsequently found widely distributed in tissues (*8*) and in very high concentrations in platelets (*8, 9*). Evidence that TGF-β may be important in wound healing included stimulation of total protein, collagen, and DNA content in wound chambers implanted in vivo (*10*), stimulation of expression of fibronectin and collagen by fibroblast lines in tissue culture (*11*), and rapid, reversible formation of granulation tissue when injected subcutaneously into newborn mice (*12*). TGF-β also manifests growth-inhibitory properties for specific cell types (*13, 14*) and thus may serve as a bifunctional regulator of cellular growth and differentiation (*9*).

T. A. Mustoe and P. Gramates, Department of Surgery, Washington University Medical Center, St. Louis, MO 63110.
G. F. Pierce, Departments of Pathology and Medicine, Washington University School of Medicine, St. Louis, MO 63110.
A. Thomason, Amgen, Inc., Thousand Oaks, CA 91320.
M. B. Sporn, Laboratory for Chemoprevention, National Cancer Institute, National Institutes of Health, Bethesda, MD 20892.
T. F. Deuel, Departments of Medicine and Biological Chemistry, Washington University Medical Center, St. Louis, MO 63110.

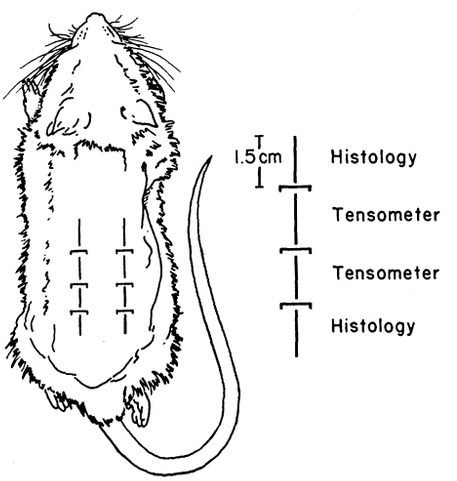

Fig. 1. Young adult male Sprague-Dawley rats, 300 to 350 g (Sasco; Omaha, Nebraska), anesthetized with pentobarbital, had 6-cm linear incisions placed through the skin 1.5 cm on either side of the midline. A bovine collagen suspension, an equal volume of saline, or nothing was applied to the sides of each incision, with each animal serving as its own control. The wounds were then coapted with three surgical clips. For study, the entire dorsal skin of the rat was excised. A template with parallel surgical blades was used to excise two 8-mm strips between clips from each incision. Histological samples were taken from the ends.

Normal wound healing is thought to occur in three phases: (i) cellular migration and inflammation for several days; (ii) proliferation of fibroblasts for 2 to 4 weeks, with new collagen synthesis; and (iii) remodeling of the scar from 1 month to 1 year, a process that includes collagen cross-linking and active collagen turnover (*15*). Increased collagen production early in wound healing is directly related to an increase in wound strength (*15*).

The most important aspect of wound healing after surgical incision is the generation of wound strength. Various measures have been used to promote surgical healing (involving asepsis, surgical technique, suture material, and the like), but no pharmacologic agent has been found to augment normal surgical wound healing. Naturally occurring growth factors are potential candidates.

In this work, a linear skin incision model was chosen to represent a true surgical wound that could be reproducibly analyzed in a nonsubjective, highly controlled manner (Fig. 1). Bovine collagen (Zyderm II; Collagen Corporation, Palo Alto, California) was selected as the vehicle in which to apply growth factor at the time of wounding because it is highly purified, hypoallergenic, and forms a viscous suspension that is easily applied to the cut edges of each incision. Collagen suspensions, when compared with saline or with no treatment, had no statistically significant effect (analysis of variance) on peak wound healing strength from postwounding day 3 to postwounding day 21 (Fig. 2A). As expected from previous studies of this model (*15*), a lag phase of about 2 days was observed before wound strength began to increase in a linear fashion; the increase in wound strength was correlated with the onset of collagen synthesis.

We began a systematic study of the effects of TGF-β in this model. When TGF-β was added to collagen suspensions (Fig. 2B), a lag phase was observed before the tensile strength of the wound increased at day 3 to levels 151% of the tensile strength of wounds not treated with TGF-β (108 ± 27 g as opposed to 72 ± 20 g, two-tailed *t* test for paired results; not significant) and to levels 221% of controls at day 5 (293 ± 48 g as opposed to 133 ± 29 g; $P = 0.01$). Statistically significant effects were seen also on days 7 and 14 after wounding. At 5 and 7 days, TGF-β–treated wounds had breaking strengths equivalent to control wounds at days 8 and 10, respectively, an indication of about a 3-day acceleration of healing in the first week. At day 7, when new collagen synthesis is occurring at a linear rate (*15*), the increase in wound strength between the treated and untreated wounds was not statistically different from the increases observed at days 5, 10, and 14 (Table 1); this observation indicated that the optimal effect of TGF-β has been achieved by days 5 to 7 and persisted through day 14.

The influence of increasing concentrations of TGF-β in collagen was then tested at day 5 after wounding (Fig. 2C). No statistically significant effect on wound healing was seen with 0.05 μg of TGF-β, whereas a highly significant effect (165% of control, 160 ± 11 g as opposed to 97 ± 10 g; $P = 0.001$) was seen with 0.25 μg. Further increases were seen with concentrations of

Table 1. The difference between individual TGF-β–treated and control wound pairs from Fig. 2B was calculated for each postwounding day and each TGF-β dose. Analysis of variance comparing differences in breaking strength on the peak day 7 to those observed on days 2, 3, 5, 10, and 14 was performed. The *P* value relative to day 7 was determined with the SAS general linear models procedure for multiple comparisons with correction for unequal variances. Significant differences were seen only when comparing differences on day 7 to those on days 2 and 3, thereby indicating a delayed but long-lasting effect of TGF-β on the increase in breaking strength that is consistent with the known kinetics of incisional model healing (*15*).

Post-wounding day	TGF-β dose per incision (μg)	Difference in maximum breaking strength (g)	*P* value relative to day 7
7	2	196 ± 52	
2	2	9 ± 7	0.018
3	2	1 ± 17	0.009
5	2	115 ± 43*	0.287
10	2	122 ± 84	0.305
14	2	137 ± 50	0.381

*Differs from the value in Fig. 2 because only paired samples were used to calculate the difference breaking strength in this analysis.

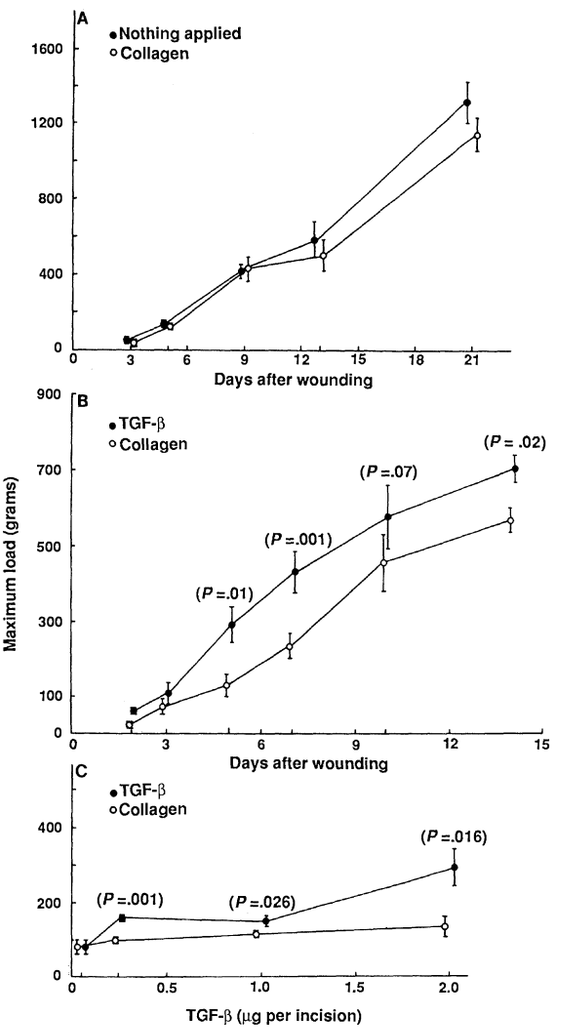

Fig. 2. The maximum load tolerated by wounds was measured with a tensometer (Tensometer 10; Monsanto, St. Louis, Missouri) on two 8-mm skin strips from each of two 6-cm wounds (one experimental, one control) per rat. Each point represents measurements made on eight wound strips from four rats. Measurements were made on strips stretched at 10 mm per minute, with the maximum load recorded on a graph. Breaking strength was not measured on wounds showing evidence of infection, excessive hemorrhage, or poor coaptation (less than 5% of all wounds). The median and mean values of tensile strength for each group were essentially identical. Results and statistical analysis are shown from one of at least three separate but essentially identical experiments for each graph. TGF-β was prepared as described (*8*) and was homogeneous when analyzed on SDS-polyacrylamide gel electrophoresis (SDS-PAGE) and silver-stained. For use in wounds, it was lyophilized and reconstituted in phosphate-buffered saline, *p*H 7.4. The *p*H of the TGF-β after it was mixed with collagen remained above 7. (**A**) Skin strips were harvested at various days after wounding. The effect of collagen diluted in saline applied to the incisions at the time of wounding (10 mg/ml) (○) was compared to wounds receiving no treatment (●). Results with saline alone were identical to these curves. No significant differences were observed. Means ± SEM are presented. (**B**) Collagen (10 mg/ml) was applied to wounds with (●) or without (○) TGF-β (2 μg per incision), and skin strips were removed at the days shown. *P* values derived from analysis of variance (ANOVA) show comparisons of individual experimental and control points with respect to the entire curve. (**C**) A TGF-β dose-response curve was obtained for wounds harvested 5 days after wounding and compared to collagen alone (10 mg/ml). *P* values are based on comparisons of individual points. TGF-β was tested at 0.05, 0.25, 1, and 2 μg per incision.

TGF-β of 1 μg and 2 μg (both statistically significant), although these increases in tensile strength were not precisely linear with TGF-β concentrations. Control wounds from these different TGF-β treatment groups had nearly identical breaking strengths (Fig. 2C), an indication that the TGF-β effect is limited to the area of local application. When TGF-β in a saline vehicle was applied to wounds, the tensile strength of the wounds did not increase; collagen thus appears to be a slow-release vehicle that resulted in prolonged local exposure of wounds to TGF-β. Bovine serum albumin was added to the collagen vehicle in concentrations up to 40 μg per incision. No differences in breaking strength were observed in comparison with suspensions of collagen in phosphate-buffered saline (PBS) or saline alone.

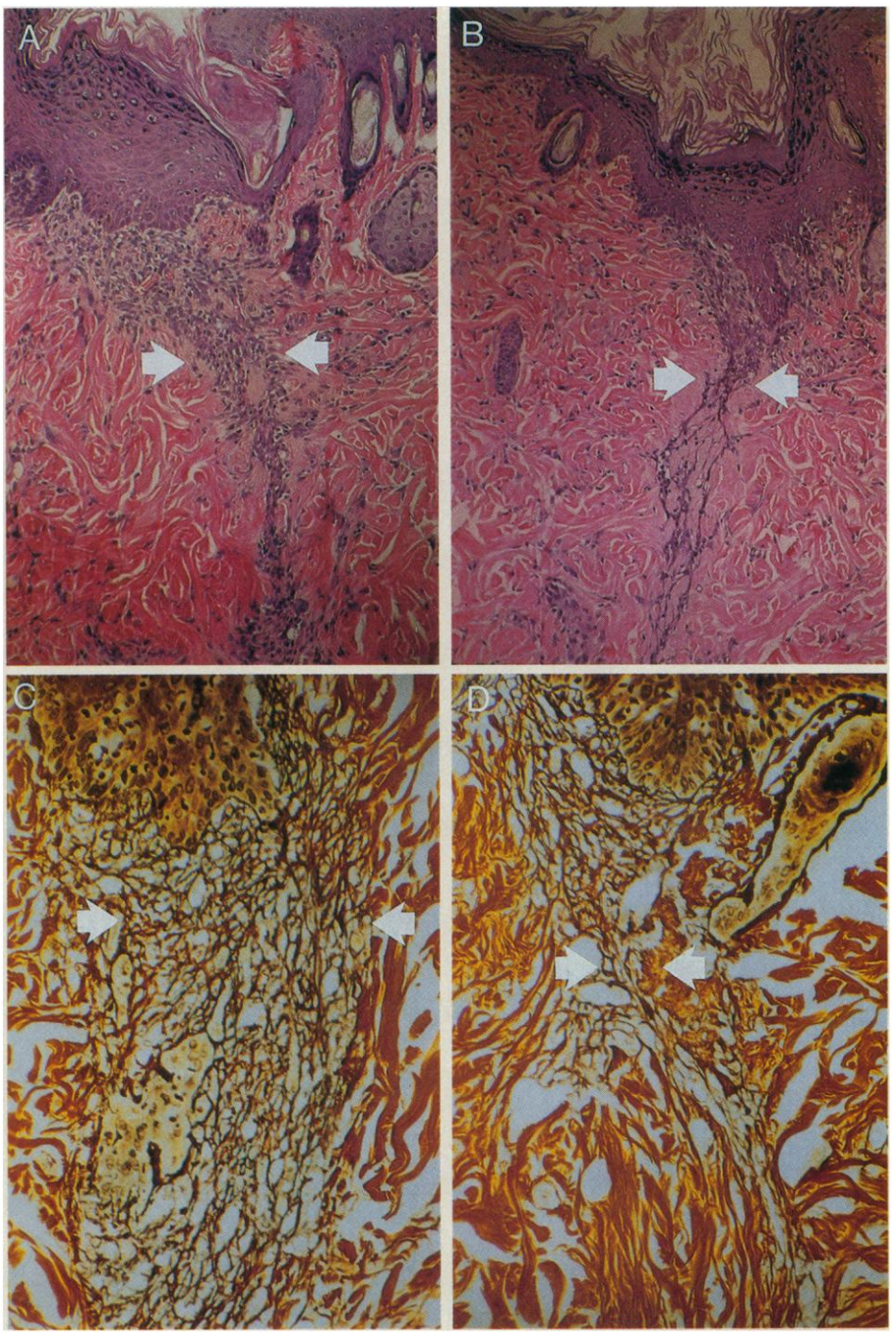

Fig. 3. (**A** and **B**) Hematoxylin and eosin stain (magnification, ×100) and (**C** and **D**) reticulin stain (×200) of parallel incisions harvested on the fifth day after wounding. Collagen plus TGF-β (2 μg) (A and C) or collagen alone (B and D) was applied at the time of wounding. Samples were taken from the end quadrants of each wound and were placed immediately in phosphate-buffered Formalin (10%). Middle quadrants were used for tensometry. Wounds from eight rats treated with TGF-β in different experiments showed similar histological results in comparison to control wounds. The wounds treated with TGF-β show a cellular infiltrate extending through the wound (arrows) to the base and consisting primarily of fibroblasts and monocytes at this stage. New reticulin fibers are evident in TGF-β–treated wounds but not in control wounds (arrows).

Histological sections were examined to correlate the tensile strength measurements with a morphological analysis of the treated wounds. The TGF-β–treated wounds showed a much greater influx of mononuclear cells and fibroblasts than was seen in the collagen controls (Fig. 3, A and B). The cellular infiltrate in treated wounds was accompanied by a striking increase in new collagen production, as assessed by the reticulin stain (Fig. 3, C and D), which identifies predominantly newly synthesized collagen that is not cross-linked.

Our results show that TGF-β can significantly accelerate wound healing in vivo. Acceleration of surgical wound healing during the critical early phases was associated with a single application of this pharmacologic agent. These results were consistently reproducible and statistically significant when compared to control wounds.

The effects of TGF-β on wound strength in the early postwounding phase coincided with a marked cellular influx and with new collagen synthesis. Thus, TGF-β may directly stimulate chemotaxis and collagen synthesis in vivo, as demonstrated previously in vitro and in wound chamber models (*10–12*).

REFERENCES AND NOTES

1. T. F. Deuel, S. S. Huang, J. S. Huang, in *Biochemistry of Platelets*, D. R. Phillips and M. A. Shuman, Eds. (Academic Press, New York, 1986), pp. 347–375.
2. M. A. Packham, E. E. Nishizawa, J. F. Mustard, *Biochem. Pharmacol.* (Suppl.) (March 1968); p. 171; R. L. Nachman, B. Weksler, B. Ferris, *J. Clin. Invest.* **51**, 549 (1972).
3. J. G. Hirsch, *J. Exp. Med.* **112**, 15 (1960); B. B. Weksler and C. E. Coupal, *ibid.* **137**, 1419 (1973).
4. T. F. Deuel, R. M. Senior, J. S. Huang, G. L. Griffin, *J. Clin. Invest.* **69**, 1046 (1982); J. S. Huang, S. S. Huang, T. F. Deuel, *J. Cell Biol.* **97**, 383 (1983).
5. G. R. Grotendorst, H. E. J. Seppa, H. K. Kleinman, G. R. Martin, *Proc. Natl. Acad. Sci. U.S.A.* **78**, 3669 (1981); H. E. J. Seppa, G. R. Grotendorst, S. Seppa, E. Schiffmann, G. R. Martin, *J. Cell Biol.* **92**, 584 (1982); R. M. Senior, G. L. Griffin, J. S. Huang, D. A. Walz, T. F. Deuel, *ibid.* **96**, 382 (1983).
6. D. Y. Tzeng *et al.*, *Blood* **64**, 1123 (1984); D. Y. Tzeng, T. F. Deuel, J. S. Huang, R. L. Baehner, *ibid.* **66**, 179 (1985); E. A. Bauer, T. W. Cooper, J. S. Huang, J. Altman, T. F. Deuel, *Proc. Natl. Acad. Sci. U.S.A.* **82**, 4132 (1985).
7. J. E. DeLarco and G. J. Todaro, *Proc. Natl. Acad. Sci. U.S.A.* **75**, 4001 (1978); A. B. Roberts *et al.*, *ibid.* 77, 3494 (1980).
8. A. B. Roberts, M. A. Anzano, L. C. Lamb, J. M. Smith, M. B. Sporn, *ibid.* **78**, 5339 (1981); R. K. Assoian, A. Komoriya, C. A. Meyers, D. M. Miller, M. B. Sporn, *J. Biol. Chem.* **258**, 7155 (1983).
9. C. B. Childs, J. A. Proper, R. F. Tucker, H. L. Moses, *Proc. Natl. Acad. Sci. U.S.A.* **79**, 5312 (1982); R. K. Assoian and M. B. Sporn, *J. Cell Biol.* **102**, 1217 (1986); M. B. Sporn, A. B. Roberts, L.

M. Wakefield, R. K. Assoian, *Science* **233**, 532 (1986).
10. M. B. Sporn *et al.*, *Science* **219**, 1329 (1983); W. T. Lawrence *et al.*, *Ann. Surg.* **203**, 142 (1986).
11. R. A. Ignotz and J. Massague, *J. Biol. Chem.* **261**, 4337 (1986).
12. A. B. Roberts *et al.*, *Proc. Natl. Acad. Sci. U.S.A.* **83**, 4167 (1986).
13. R. L. Heimark, D. R. Twardzik, S. M. Schwartz, *Science* **233**, 1078 (1986); J. Massagué *et al.*, *Proc. Natl. Acad. Sci. U.S.A.* **83**, 8206 (1986); J. H. Kehrl *et al.*, *J. Exp. Med.* **163**, 1037 (1986).
14. G. D. Shipley *et al.*, *Cancer Res.* **44**, 710 (1984); G. D. Shipley, R. F. Tucker, H. L. Moses, *Proc. Natl. Acad. Sci. U.S.A.* **82**, 4147 (1985).
15. R. Ross, *Biol. Rev. (Cambridge)* **43**, 51 (1968); E. E. Peacock, in *Wound Repair* (Saunders, Philadelphia, ed. 3, 1984), pp. 102–140.
16. We thank J. Reed, J. Lingelbach, and O. Kendrick for excellent technical assistance; J. Smith and L. Dart for preparation of TGF-β from platelets; W. Seyfried, Division of Biostatistics, Washington University Medical School, for statistical assistance; E. Miller and the Jewish Hospital histology laboratory for skillful services; and E. Crouch, Department of Pathology, Jewish Hospital, for helpful discussions.

19 December 1986; accepted 19 June 1987

IRAS Serendipitous Survey Observations of Pluto and Charon

MARK V. SYKES, ROC M. CUTRI, LARRY A. LEBOFSKY, RICHARD P. BINZEL

On 16 August 1983 the Infrared Astronomical Satellite made two separate pointed observations of Pluto and its moon Charon. Because of the small angular displacement of the system between the times of measurement, the Pluto-Charon system was identified as a source in the Serendipitous Survey (SSC 14029+0518). Detections were made at 60 and 100 micrometers with color-corrected flux densities of 581 ± 58 and 721 ± 123 millijanskys, respectively. Pluto is best described as having a dark equatorial band, and brighter polar caps of methane ice extending to ±45° latitude, at most. An upper limit of approximately 9 meter-amagats is placed on the column abundance of a methane atmosphere on Pluto, which is comparable to recent upper limits based on independent ground-based spectroscopy.

THERE HAS BEEN A SURGE OF INTEREST in Pluto in recent years, primarily because of the discovery of its moon Charon (*1*) and the advent of mutual eclipses between the two bodies as Earth passes through the projected orbital plane of Charon (*2*). These eclipse observations will allow for accurate determination of the radii and geometric albedos of Pluto and Charon, as well as the mapping of darker and lighter areas on their surfaces. More interest was generated when a methane atmosphere on Pluto was reported with a column abundance of 27 m-A (*3*), on the basis of ground-based spectroscopy (*4*). Although more recent ground-based observations and analyses have reduced this value by factors of 2 to 4 (*5, 6*), a "significant" atmosphere was reported on the basis of observations made by the Infrared Astronomical Satellite (IRAS) during a survey of the sky at thermal infrared wavelengths (*7*). In this report we analyze more sensitive "pointed" observations made of Pluto by IRAS (*8*), and present quantitative limits on the Pluto atmosphere by means of infrared observations. We conclude that the atmosphere is thinner than originally thought (consistent with the recent ground-based observations) and that surface methane ice is restricted to ice caps whose locations vary in response to large changes in subsolar latitude over a Pluto year (248 Earth years).

Two separate pointed observations were made of the fields around Pluto on 16 August 1983 at approximately 0430 UT and 1130 UT, in four broad passbands centered on 12, 25, 60, and 100 μm. The images reconstructed from the scans are shown in Fig. 1, and information regarding the Pluto-Charon system at the mean time of observation is given in Table 1. The IRAS Serendipitous Survey examined the point sources extracted from nearly all pointed observation fields that were observed at least twice during the satellite's mission. Infrared sources that were found to lie at nearly the same position and have similar flux densities in two observations of the same field were considered "confirmed" and were compiled in the IRAS Serendipitous Survey Catalog (SSC) (*9*).

A comparison of Pluto's ephemeris position with all of the SSC sources in the Pluto AO fields (Table 2) confirmed the identification of the brightest source (H) seen at 60 and 100 μm as being the Pluto-Charon system (SSC 14029+0518) (*10*). The color-corrected 60- and 100-μm flux densities are 581 ± 58 mJy and 721 ± 123 mJy, respectively (*11*).

Figure 2 shows the Palomar Sky Survey red-plate image in the region of the pointed observation field with the approximate location and uncertainty box of each source indicated. Pluto was not overlying any previously known source that would have contributed to the observed flux at IRAS wavelengths. As can be seen in Fig. 1, Pluto-Charon was detected easily at 60 and 100 μm, and only upper limits are available at 12 and 25 μm (Fig. 3) on account of the large distance between Pluto and the sun. The thermal flux density (B_ν) of a blackbody in radiative equilibrium with sunlight at Pluto's heliocentric distance ($T \sim 51$ K) would peak at around 100 μm and decrease exponentially at shorter wavelengths. Other sources found in the Pluto field (Fig. 2) include two SAO stars (C and D), several faint galaxies (A, B, E, and F), and two sources that are likely associated with modulations in the extended infrared cirrus emission (G and I).

Pluto was also observed while IRAS was in the survey mode (*7*), but a detection was made only at 60 μm. The flux density reported (420 mJy) was much smaller than the value derived from the SSC (Fig. 3). In part, this is probably a result of the lower

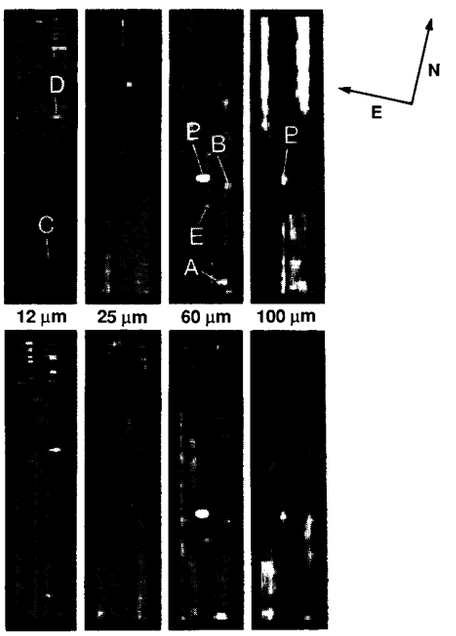

Fig. 1. IRAS observations of the Pluto field taken in the pointed mode on 16 August 1983. Two separate scans (**top** and **bottom**) were taken ~7 hours apart. Several of the SSC sources are clearly seen and marked by their letter designations (Table 2). Pluto-Charon (P) is seen as a strong source at 60 and 100 μm but is invisible at the shorter wavelengths. The only sources seen at 12 μm are SAO stars. At 100 μm, evidence for extended infrared cirrus emission can be seen.

M. V. Sykes and R. M. Cutri, Steward Observatory, University of Arizona, Tucson, AZ 85721.
L. A. Lebofsky, Lunar and Planetary Laboratory, University of Arizona, Tucson, AZ 85721.
R. P. Binzel, Planetary Science Institute, Tucson, AZ 85719.